NURETH14-183

PARTICLE PRECIPITATION AND MIXING SIMULATED BY RIGID DYNAMIC-MOVING PARTICLE SEMI-IMPLICIT (RD-MPS) METHOD

S. Park¹, H. S. Park^{2*}, G. Jeun³ and B. J. Cho¹
KEPCO Nuclear Fuel, Daejeon, Republic of Korea
² SINEWSTEK, Solna, Stockholm, Sweden
³ Hanyang University, Seoul, Republic of Korea

* Corresponding authors

Abstract

The particle precipitation and mixing related to the corium debris bed formation and coolability in severe accidents are investigated by using a new CFD tool, called the ADDA code. The code is developed based on an enhanced particle method which combines the MPS (Moving Particle Semi-implicit) algorithm with the rigid body dynamics method. The analysis successively simulates the entire process of debris bed formation which includes corium jet breakup, mixing, and sedimentation to identify the key characteristics to form the corium debris bed with coolable configurations. The 2-D and 3-D simulation re-created the detailed flow structures and mixing phenomena and final sedimentation process. For the analysis of the debris formation, it is suggested that the full 3-D simulation provides more accurate prediction than ones from the 2-D simulations since the debris formation largely depends on the process of particle precipitation and mixing phenomena prior to its settlement.

1. Introduction

Particle dissipation and mixing in liquid is common multiphase phenomena in nature and industrial processes. It is also one of important phenomena in nuclear safety analysis which involves severe accidents associated with corium after a complete or prolonged lack of cooling as witnessed in the Fukushima accident after beyond design-based magnitudes of combined natural disasters of earthquake and tsunami.

To terminate or mitigate the accident progression towards the exposure of radioactive materials to the environment after the failure of several defense-in-depth barriers due to the molten corium-coolant-structure interactions (CCSI), it is essential to assure that the corium be stabilized and become coolable at any circumstances. During the core melting, the corium relocated from the reactor core to the bottom of the reactor vessel (in-vessel) or to the bottom of the reactor cavity (ex-vessel) if reactor vessel failures interacts with residual water and becomes small fragmented debris.

If in the process no or insignificant energetic fuel-coolant interaction (FCI) takes place, a stream of corium break up into small fragments or debris (order of mm to cm in diameter) due to dynamic interaction with surrounding single or two-phase coolant. The fragments with the decay heat generation are mixed with the coolant and sediment on the bottom of the reactor cavity floor in the case of an ex-vessel severe accident progression scenario, forming an agglomerated porous

debris bed [1][2]. The self-heating hot corium debris can be re-melted and create a pool of molten corium on the concrete cavity floor if it is not able to be cooled by the surrounding flooded coolant. It eventually causes the concrete floor erosion due to the molten corium concrete interactions (MCCI) which threatens the final barrier of the defense-in-depth measures, the containment.

Therefore, the coolability of corium debris beds has also actively studied and has extensive literatures and experimental database [3]. It is crucial to understand what the coolable configuration of the debris bed is and how the configuration can be formed to ensure the selfsustainable long-term cooling of the corium debris bed. To answer those questions, number of associated multiphase fluid dynamic and heat transfer phenomena should be addressed such as (a) corium jet breakup and mixing, (b) corium debris sedimentation and agglomeration and (c) fluid flow in porous media. Concerning the corium jet breakup and mixing, several decades long intensive research efforts have been carried out in lights of energetic fuel-coolant interaction in where the jet breakup and mixing phenomena are the pre-conditions of the subsequent steam explosion and dynamic loading to surrounding structures [4]. Conventional studies on the multiphase phenomena in the porous media have also very extend information in petroleum industry [5]. However, there are relatively limited research on the debris sedimentation and agglomeration in the perspective of corium coolability [3]. To draw reasonable conclusions on the debris bed coolability issues, the characteristics of the porous debris bed such local porosity distribution, debris bed formation, particle size distribution, porous structure etc, determined by the entire jet break-up, precipitation, and mixing process as key parameters should be understood. Recent research activities on the corium coolability address the issues experimentally [6] and analytically [7]. In experiments, however, the end state of the debris formation after the FCI processes is often obtained. Some of visualization techniques allow understanding the dynamics mixing and precipitation process during FCIs which hints the evolving mechanism for the end state debris bed formed. Therefore, advanced computational fluid dynamic techniques which handle such multiphase phenomena are often to be supplementary tools to understand the phenomena.

The computational methods used to simulate the multiphase and multi-component flow [8] can be categorized into two general classes; conventional continuum methods and particle methods. Hybrid particle-continuum methods [9] are also popularly used for the dispersed particle flow in the continuous flow such as particle precipitation and agglomeration phenomena to utilize the benefit of both continuum and particle methods. In general, the particle methods [10] for simulation of multiphase and multi-component flow raised in nuclear safety analysis are computationally inefficient relative to continuum methods and needed to be calibrated. However, there are also some rewarding benefits to use the methods because of no need of interface capturing, rigorous mass conservation, relatively simply simulation of complex physical processes and so on.

In this paper, therefore, accompanying with experimental efforts, a new multiphase computational fluid dynamic (MCFD) tool called ADDA (Analysis of Debris Dynamics and Agglomeration) [11], based on the particle method is used to simulate the entire process of debris bed formation including corium jet breakup, mixing, and sedimentation and to identify the key characteristics to form the corium debris bed with coolable configurations. The algorithm of the ADDA code is originally based on the moving particle semi-implicit (MPS) method [12][13][14]

and has an inherent ability to simulate multiphase dynamics using groups of particles which simulate fluid momentum transfers by particle collision among different fluids and easily handle the interface of multiphase of fluids. The code has been enhanced by employing a new MPS algorithm [16] developed by integrating the original algorithm with rigid body dynamics improving its numeric stability by enhancing the incompressibility of fluid and thus enabling to simulate the entire jet mixing process starting from jet entrance into liquid and jet break-up, to particle agglomeration. For the code validation, the QUESO experiment [17][18] designed to test the heat and momentum transfer models in the FCI multi-filed codes and verifying the capability of the FCI codes was chosen because the experiment employed a pack of well-defined spherical particles to emulate the corium jet, simulating FCI pre-mixing conditions with known fragment diameters with detailed measurement of pressure, temperature and steaming rates during the pre-mixing process.

2. The Analysis of Debris Dynamics and Agglomeration (ADDA) Code

The detailed descriptions and formulations on the MPS method [12][13][14] and the rigid body dynamics [15] as well as on the enhanced MPS [16] are well documented in the references. In this section, the basic principle of the ADDA algorithm will be briefly described.

2.1 Moving Particle Semi-Implicit Method (MPS)

Mass and momentum equations for incompressible flows in the ADDA code are expressed as

$$\frac{\partial \rho}{\partial t} + \nabla \cdot (\rho \mathbf{u}) = 0 \tag{1}$$

$$\rho \frac{D\mathbf{u}}{Dt} = -\nabla P + \mu \nabla^2 \mathbf{u} + \rho g + \sigma \kappa \delta \hat{\mathbf{n}}, \tag{2}$$

where D/Dt means the Lagrangian differential operator, ρ is density, \mathbf{u} is velocity, t is time, P is pressure, μ is the viscosity coefficient, g is the acceleration due to gravity, σ is surface tension coefficient, κ is the curvature of the surface, δ is the delta function, and $\hat{\mathbf{n}}$ is a unit vector normal to the interface.

The MPS method represents a fluid motion by moving particles. All the interactions are limited to neighboring particles covered with a distance weight function as

$$w(r) = \begin{cases} \frac{r_e}{r} - 1, & 0 \le r \le r_e, \\ 0, & r \ge r_e, \end{cases}$$

$$(3)$$

where r_e is the radius of the interaction area ($r_e = 2.1 \, \zeta_0$ in this study), ζ_0 represents the distance between adjacent particles in the initial arrangement, and r is the distance between two particles i and j.

$$r = \left| \mathbf{r}_{j} - \mathbf{r}_{i} \right| \tag{4}$$

The weight function is zero when r is longer than r_e .

Summation of the weight functions for the particle i is called particle number density, n_i , which is used as a normalization factor for averaging:

$$n_i = \sum_{j \neq i} w(|\mathbf{r}_j - \mathbf{r}_i|) \tag{5}$$

The particle number density is proportional to the fluid density. It should be constant for incompressible flows: $n_i = n^0$, where n^0 is dependent on the initial arrangement of particles.

Gradient and Laplacian operators involved in the governing equations are transformed to equivalent particle interactions. If φ is an arbitrary scalar, particle interaction models for differential operators are expressed as

$$\langle \nabla \phi \rangle_i = \frac{d}{n^0} \sum_{j \neq i} \left[\frac{\phi_j - \phi_i}{|\mathbf{r}_i - \mathbf{r}_i|^2} (\mathbf{r}_j - \mathbf{r}_i) w(|\mathbf{r}_j - \mathbf{r}_i|) \right]$$
(6)

$$\langle \nabla^2 \phi \rangle_i = \frac{2d}{\lambda_i n^0} \sum_{i \neq i} \left[(\phi_i - \phi_i) w(|\mathbf{r}_i - \mathbf{r}_i|) \right]$$
(7)

where d is the number of space dimensions and λ_i is defined as

$$\lambda_{i} = \frac{\sum_{i \neq j} |\mathbf{r}_{j} - \mathbf{r}_{i}|^{2} w(|\mathbf{r}_{j} - \mathbf{r}_{i}|)}{\sum_{i \neq j} w(|\mathbf{r}_{j} - \mathbf{r}_{i}|)}$$
(8)

The gradient model is obtained from the average of gradient vectors, which are determined between a particle, i and its neighboring particles j_s . The Laplacian model is derived from the physical concept of diffusion. The parameter λ_i is introduced to make the variance increase equal to that of the analytical solution. Substituting the above particle interaction models into the governing equations, (Eqs. 1 and 2), we can obtain the particle dynamics to simulate fluid flows.

2.2 Non-Penetrating Rigid Body Dynamics Model

The MPS method described in the previous section easily handle multiphase flow in a fully Lagrangian way with a particle which has no mass or volume but related to other particles by a weight functions (Eq. 3) defined in terms of the distance between two particles. This core concept allows this particle method to simulate continuous liquid flow. However, the method experiences some numerical instability in simulating multiphase flow when (1) fluid particles approach each other too close, resulting in their weight functions become too large and (2) interfaces in multiphase flow are not clearly sustained. To overcome these shortcomings, the incompressibility of the fluid particles should be maintained in any circumstances and also the mechanical energy transfer between the different fluids should be well preserved at the interface of the fluids. In so doing, the concept of the non-penetrating rigid body dynamics is coupled with the original MPS methods to increase the stability of the calculations, especially for the multiphase fluid flow.

The motions of rigid bodies obey Newtonian dynamics. To calculate the motion of a rigid particle, its position, x(t), orientation, R(t), linear momentum, P(t), and angular momentum, L(t), are needed during the calculations. Also, constant properties, like the mass of a particle, M, and the

body-space inertia tensor, I_{body} , are also needed. The remaining auxiliary quantities, I(t), $\omega(t)$ and v(t) and their definitions are stated as

$$\mathbf{v}(t) = \frac{P(t)}{M}, \quad \mathbf{I}(t) = \mathbf{R}(t)\mathbf{I}_{body}\mathbf{R}(t)^{T}, \quad \mathbf{\omega}(t) = \mathbf{I}(t)^{-1}\mathbf{L}(t)$$
(9)

where v(t) is the velocity of a particle, I(t) is the world-space inertia tensor, and $\omega(t)$ is the angular velocity at time t. The derivative relation of the above variables and constants are

$$\frac{\mathbf{x}(t)}{dt} = \mathbf{v}(t), \quad \frac{\mathbf{R}(t)}{dt} = \mathbf{\omega}(t) \times \mathbf{R}(t), \quad \frac{\mathbf{P}(t)}{dt} = \mathbf{F}(t), \quad \frac{\mathbf{L}(t)}{dt} = \mathbf{\tau}(t)$$
 (10)

where τ is the torque of a particle.

2.3 Computational Algorithm

At the stage of initializing particle configurations, initial velocities, positions, and pressures are specified. A particle diameter for the rigid body dynamics calculation is set to 0.9 ζ_o where ζ_o is the initial distance between particles. If the diameter is set to the same as ζ_o , the fluid particles constantly conflict with each other and the contact point calculations become unstable. If the diameter is much smaller than 0.9 ζ_o , the incompressibility is not well conserved and the overall calculation becomes identical to the result calculated only by the MPS method.

The ADDA calculation procedure is divided into two stages for each time step. The first step is the MPS calculation in which external forces induced by gravity, surface tension, and viscosity are calculated into temporal velocities and the pressure Poisson matrix is iteratively solved. The particle motion information obtained from the first step, i.e., \mathbf{u}_i^{**} , \mathbf{r}_i^{**} , and P_i^{**} is transferred to the rigid body dynamics calculation for the second stage. In the dynamics calculation, the velocity change generated by the MPS calculation is converted to the force as

$$\mathbf{F} = \frac{m_i \left(\mathbf{u}_i^{**} - \mathbf{u}_i^n \right)}{\Delta t} \tag{11}$$

Using the above forces acting on each fluid particle's center of mass, the colliding contacts and the resting contacts are calculated to obtain the velocities of the next time step.

By the explicit combination of rigid body dynamics and the MPS method, the stability of fluid particle simulation can be considerably improved. The compressibility of fluid can be firmly maintained since each particle cannot come close to another particle due to the rigid body dynamics calculation, In addition, the kinetic energy before and after the contact of two particles, is preserved by the rigid body dynamics model.

3. The QUEOS Experiments in FzK, Germany

For the code validation, the QUEOS experiment [17][18] designed to investigate physical phenomena (heat and momentum transfer) involved in the premixing stage of FCIs with known fragmented fuel debris size is chosen. The facility consists of the test vessel, the furnace and the valve system which separates the test vessel and the furnace system. The spheres are heated in an electric radiation furnace in an argon atmosphere to avoid the sphere surface oxidation during

heating process which alters the heat transfer during FCIs. After the pneumatically activated release of the spheres, they fall onto a heat-resistant sliding door valve and stay there for less than one second. During this time the top valve is closed to provide the gas tightness and the lower one is opened. At the same time a pressure relief valve above the middle valve is opened to release the pressure which is built up due to the heat up of the gas above the spheres. Then the middle valve opens symmetrically to two sides within 40 ms and the spheres are discharged into the water with a drop height of 0.13 m. The diameter of the sphere stream is 0.18 or 0.1 m, respectively, after the discharge from the middle valve and the spheres fall freely.

		Experimental Conditions		
		Q20	Q21	Q22
Material	-	ZrO2	ZrO2	ZrO2
Sphere Diameter	mm	4.95	4.95	4.95
Jet Diameter	mm	100	100	100
Mass	kg	7	7	14
Volume	cm ³	1830	1830	3660
No. of Sphere		18140	18140	36280
Water Temperature	°C	20	95	20
Sphere Temperature	°C	27	27	27
Duration of Pour	ms (±5)	55	55	108
Length of Pour	ms (±3)	27	27	53
Ave. Volume Faction	% (±0.01)	53	53	55

Table 1 Experimental conditions and configuration for the QUEOS Cold Tests

The water vessel made of stainless steel frames and glass has a square cross section of 0.7 m each side and a vessel height of 1.38 m. Three walls have glass windows, with a field of view of 500 by 1135 mm. A reference grid of 100x100 mm is installed close to the inside of each window. The fourth wall made of steel is prepared for the instrumentation.

Since the prime objective of the present verification is to simulate the hydrodynamic interactions among solid and liquid particles in the processes of jet breakup, mixing, precipitation and final sedimentation. For the purpose, non-boiling tests in the QUEOS experiments, Q20, Q21 and Q22 as listed in Table 1 at the ambient temperature of spheres and water temperature of 99°C are selected. Among them, in the Q21 test, a total of about 18000 ZrO₂ particles with a particle diameter of 4.95 mm in a shape of a jet with a diameter of 100 mm and a corresponding mass of 7 kg and a volume of 1830 cm³ were injected into a water pool for 55±5 ms, resulting the jet length of 270±30 mm.

4. Results and Discussions

The initial configurations of the ADDA simulation for the Q21 test in the QUEOS experiments are set as shown in Figure 1. The width of the test section is 0.7 m and the water level is 1 m. The initial distance between particles, ζ_0 , is set to be 0.013 m, the radius of interaction, r_e , is 2.1

 ζ_0 and the kernel size for Laplacian is $4.0\zeta_0$. The density of water is 1000 kg/m^3 , viscosity of water is 1.09 mPa-s, the surface tension coefficient of water is 72.8 mN/m, and the friction coefficient of ZrO_2 particle is set to 1.0. For the two-dimensional equivalent geometry, the mass of a particle is set to 0.097 kg. The initial downward velocity of the particles is 5.05 m/s.

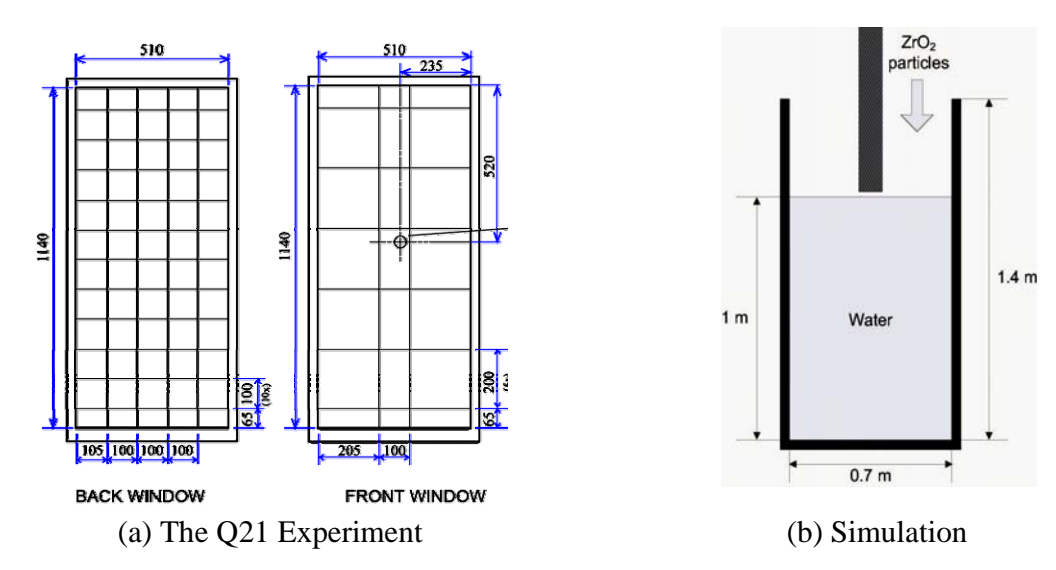


Figure 1 Schematics of the Q21 test section (from [16]) and the corresponding simulation configuration

4.1 The ADDA Simulations

4.1.1 The 2D Simulations

Figure 2 shows the side views of the Q20 and Q21 experiments and the 2D ADDA simulation results. Compering to the previous MPS analysis [14], the ADDA simulation enables to simulate the complete process of the jet mixing phenomena from the jet penetration to the particle precipitation on the bottom of the test vessel due to its enhanced numerical stability mentioned in the previous section. This capability allows to simulation the final particle bed formation on the vessel bottom and to be compared with the experimental data, Q20 and Q21.

The comparison of the simulation with the experimental images shows the qualitative resemblance of the particle jet breakup and mixing with the surrounding liquid as shown in Figure 2. The 2-D simulation clearly re-creates the structural details and mixing behaviors of particle jet while penetrating into the liquid pool, showing the jet surface instabilities; Rayleigh-Taylor instability at the hemi-spherical shape of the jet leading edge, Kelvin-Helmholtz instability at the lateral jet surface as boundary layer stripping at the tail of the dispersing leading edge particles.

Since the calculation was performed in two dimensions, dynamics of the pool liquid and mixing of particles were quantitatively exaggerated in comparison to those in the tests. For instance, the surface water level in the experiments representing the internal flow structure induced by the plunged particle jet and the associated mixing dynamics were relatively stable than those observed in the 2D simulation.

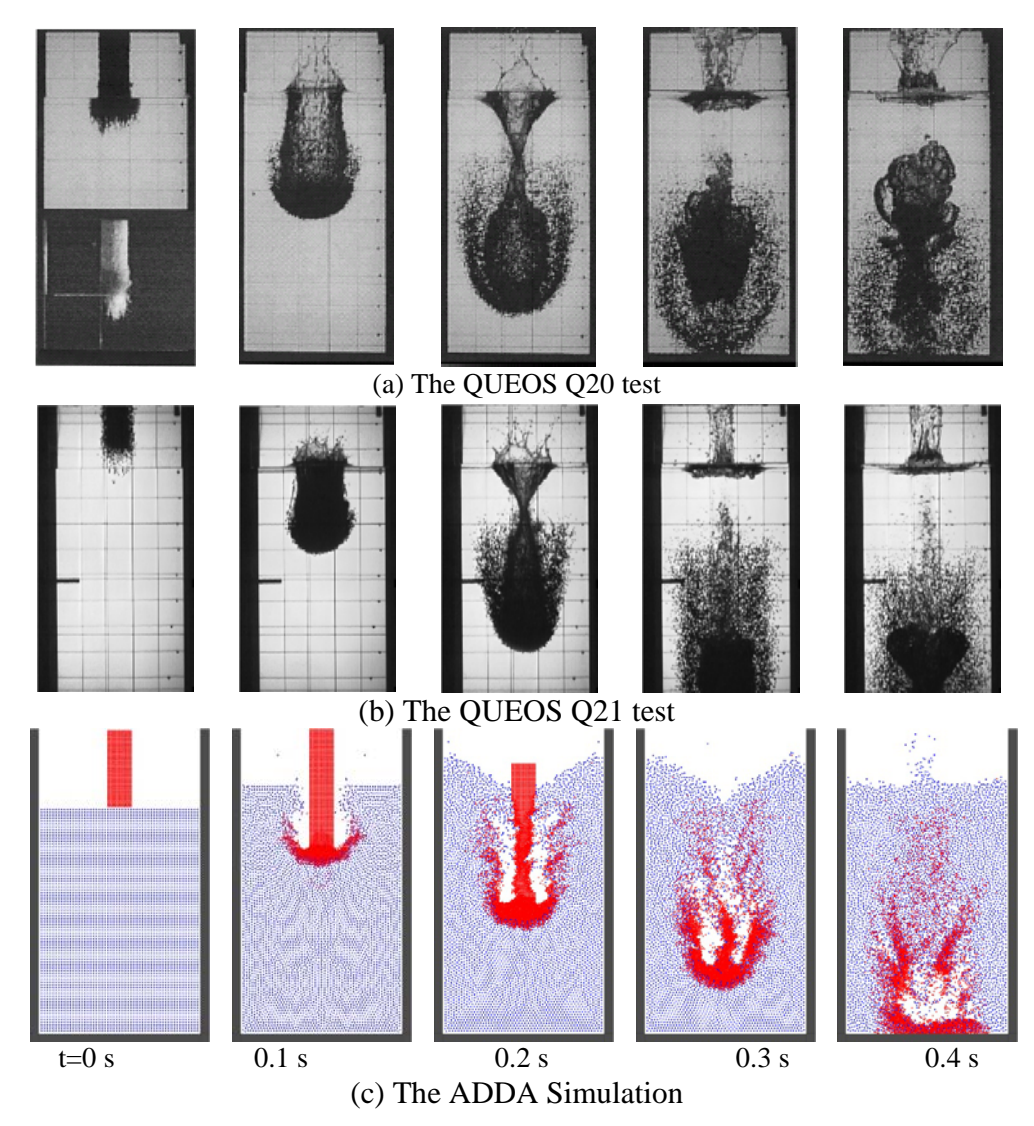


Figure 2 The 2D ADDA Simulation for the Q21 test

4.1.2 The 3D Simulations

Figure 3 illustrates the configurations of the 3D ADDA simulation for the particle jet in the Q21 test. Figure 3(a) is the actual setting for the simulation where the liquid pool in red and the particle jet in gray with liquid pool surface particles in green are visible. In order to visualize the particle jet, Figure 3(b) without the liquid pool particles is shown. Most of the analysis performed with the image data from the Figure 3(c) and 3(d) in where the general jet configurations are shown similarly to the experimental images. Those images were obtained by integrating the particles in the x-direction for the side view and the z-direction for the top view.

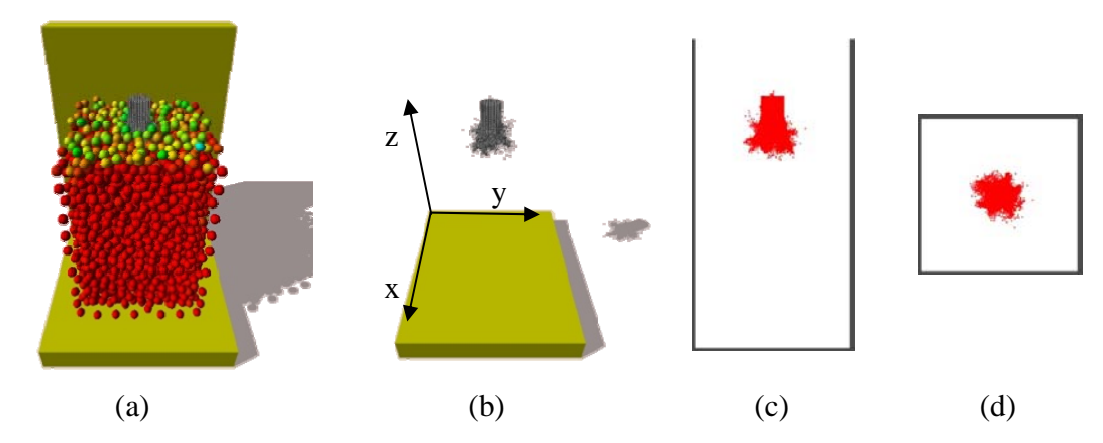


Figure 3 The 3D ADDA simulation for the Q21 test; (a) the particle jet and the liquid pool from the perspective view, (b) only the particle jet from the perspective view, (c) only particle jet from the side view and (d) only particle jet from the top view

Figure 4 compares the Q21 test with the 3D ADDA simulation, showing the overall particle precipitation during the particle jet penetration in the liquid pool. The top view of the jet shows the radial spreading of the particles.

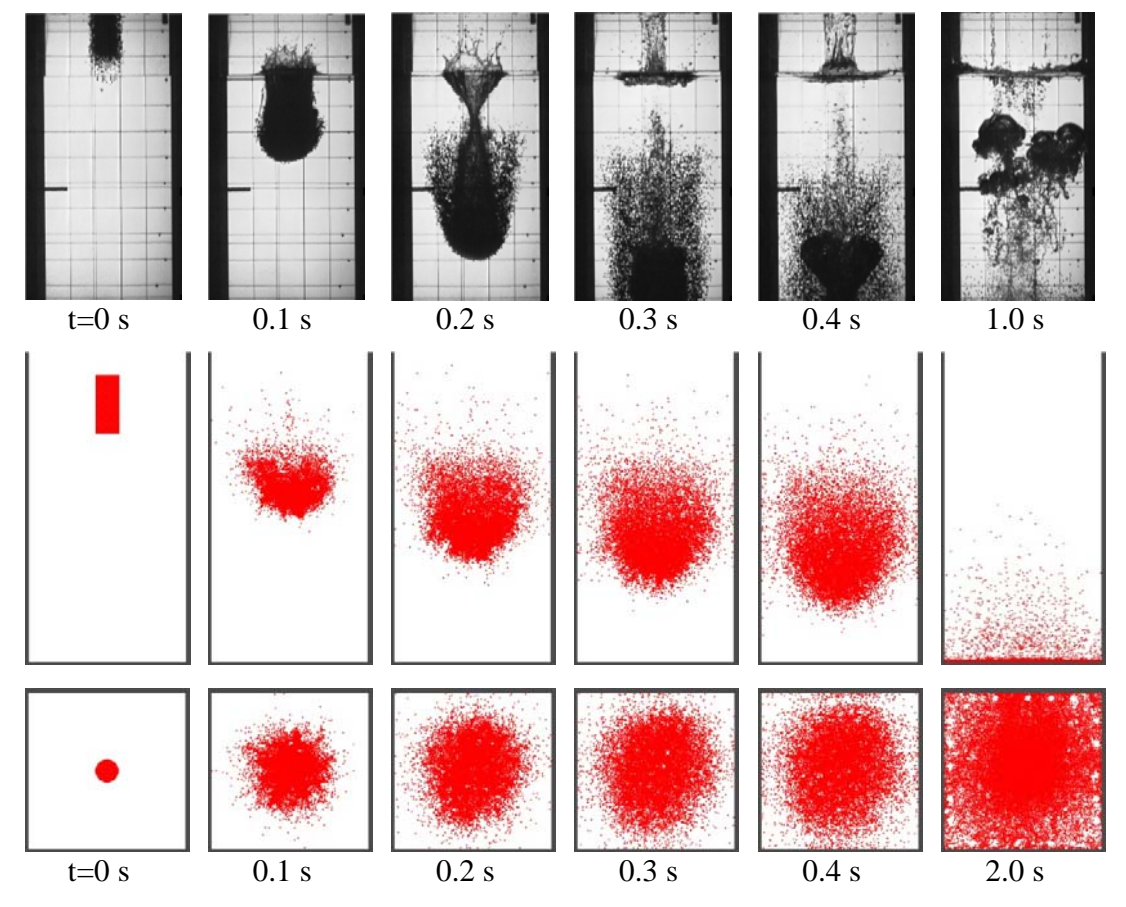


Figure 4 The 3-D ADDA Simulation for the Q21 test

4.2 Particle Jet Mixing and Precipitations

In the tests, the particle jet with the diameter of 100 mm is plunged into the liquid pool. For the Q21 test, the initial jet velocity of 5.05 m/s becomes slightly slower down to about 4.93 m/s in average prior to reach the water surface and decreases further to 3.95 m/s in average during the mixing of the particle jet with surrounding liquid until the jet leading edge reaches to the bottom of the test section at approximately 300 ms as shown in Figure 5. During the mixing phase of the jet penetration the particle jet radially disperses up to approximately 4~5 times wider than the original particle jet diameter (see t=0.3 s in Figure 5) and the dispersed particles precipitates to the bottom of the test section.

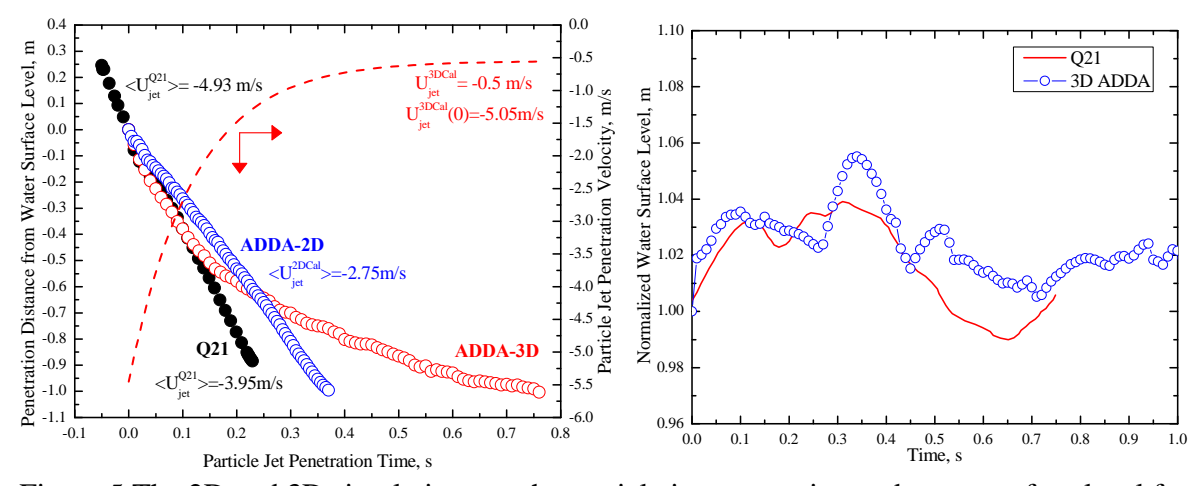


Figure 5 The 2D and 3D simulations on the particle jet penetration and water surface level for the Q21 test

The histories of the penetration length and the water surface level of the experiments and the 2D and 3D simulations are shown in Figure 5. The figure depict that the particle jet penetrations predicted by the simulation are slower in the simulations than those observed in the tests. The 3D simulation successfully calculates the initial penetration up to about 0.15s and depart from the experimental observations caused by the larger liquid pool particle diameter selected for the fast calculation. The water surface levels as an indicator for the internal liquid water pool dynamics and associated mixing between the solid particles and liquid particles for both the experiment and 3D calculation shows similar behaviors with about 6% rise in maximum. For the 2-D case, however, the water surface level was largely overestimated.

The recent experiments [6] and associated analysis [7] dedicated to the phenomena pertaining to debris coolability and formation suggested that the debris bed configurations such as debris porosity, the debris bed height and the existence of re-melted debris pool or cake significantly influenced to the debris dryout heat flux (DHF), lowering up to 50%. Those debris configurations are the function of the jet breakup and debris precipitation processes during the mixing phase of FCIs. For instances, if the liquid pool is relatively shallower than the jet breakup length, i.e., $L_p/L_b < 1$, where L_p is the pool depth and L_b is the jet breakup length, the presence of the unfragmented corium bed in a form of liquid pool or solidified cake may hinder the corium from cooling to provide the long-term stabilization and the termination of the severe accident progression.

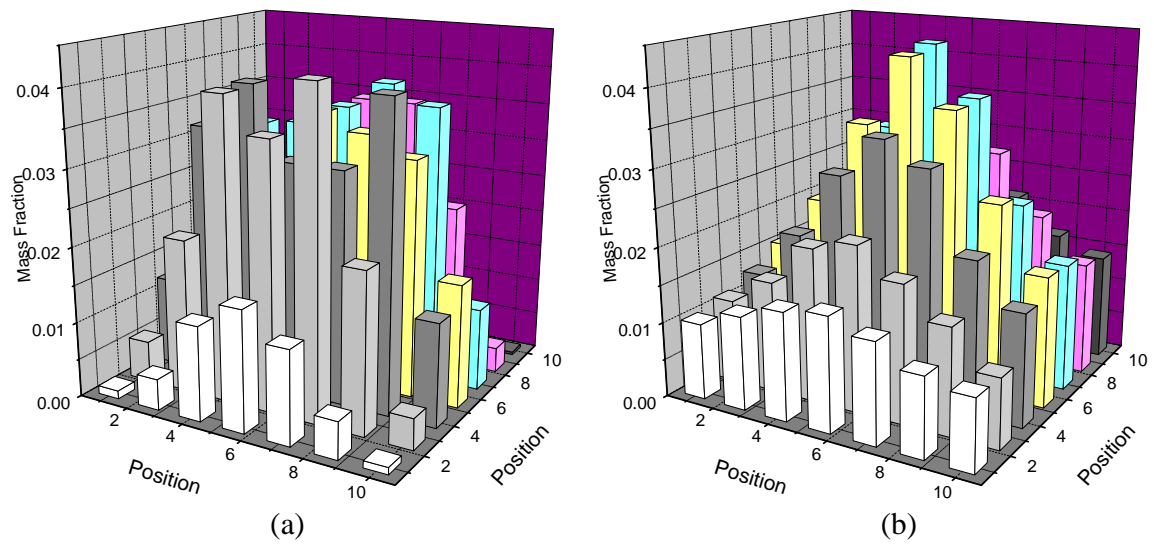


Figure 6 Normalized mass distribution of particle beds in (a) the Q21 test and (b) the 3-D ADDA simulation

4.3 Debris Bed Formation

Figure 6 plots the normalized mass distribution of spheres on the bottom of the test vessel. The accumulated sphere masses were normalized by the total sphere masses for both test and simulation results. The 3D simulation reasonably well predicted the overall shape of the particle bed, showing a dome-shape configuration with the thicker debris bed at the central regions. The maximum mass fraction at the central region was approximately 4 % out of the total mass delivered into the liquid pool.

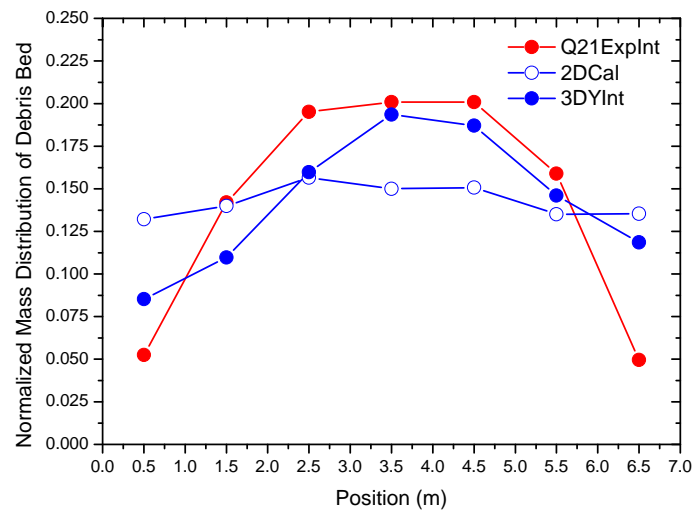


Figure 7 Normalized mass distribution of particle beds in the Q21 test and the (a) 2D and (b) 3D ADDA simulations

Figure 7 shows the normalized the mass fraction of the sediment debris bed along with the y-direction noted in Figure 3(b). In this figure, the debris bed configuration predicted by the 2D simulation become relatively flat compared to that by the 3D simulation. The 3D simulation predicted the debris bed configuration reasonably closed to the experimental observation. The strong lateral flow dynamics in the 2D simulations during the particle jet mixing and sedimentation seems responsible for the flatness of the debris bed.

The results on the particle jet penetrations, water leveling and the final debris bed formation discussed above suggest that for the particle dispersions and precipitation conceiving the debris bed formation and associated coolability analysis, the 2D simulation may be unsuitable to reasonably predict those observed in the 3-D real experiments. The speeds at the late-phase precipitation in where the 3-D simulation was departed from the experimental observation do not significantly affect to the final configuration of the debris bed.

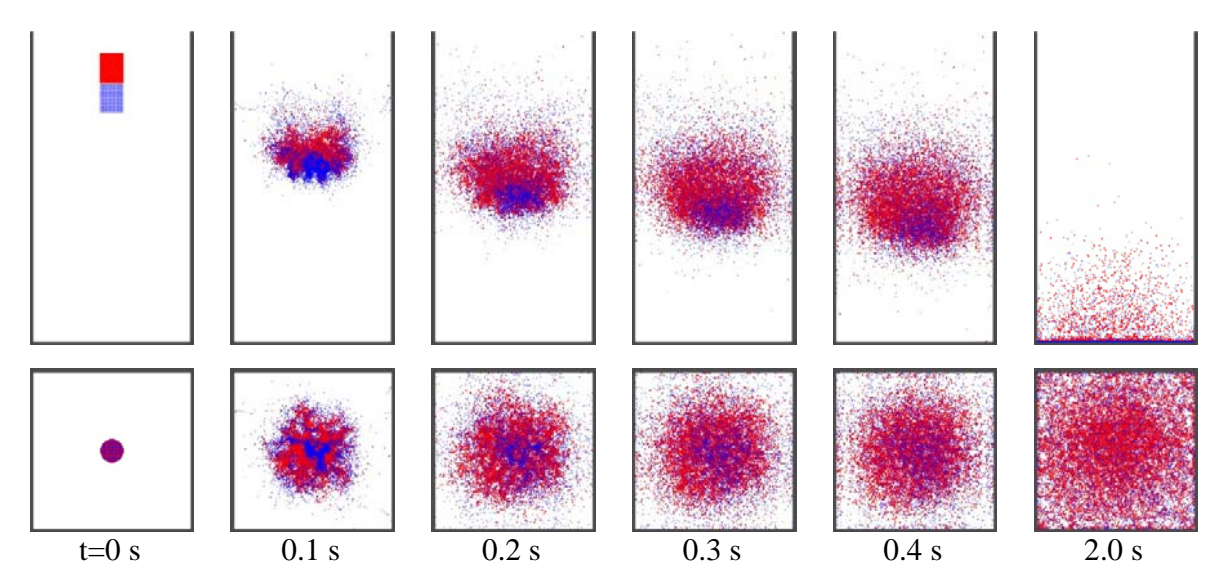


Figure 8 The 3D ADDA simulation with a two-size group particle jet

4.4 Heterogeneous Particle Jet

In order to demonstrate the potential capacity of the ADDA analysis on the debris bed formation affected by the accident scenarios, heterogeneous particle jets with different diameters was simulated. When the corium relocates into the lower plenum or reactor cavity, the corium breaks up into the debris which has ranges of size and shape distributions, leading the debris bed in a heterogeneous debris bed. Figure 8 demonstrates the particle sedimentation in where the jet fragmentation during the penetration into the liquid pool creates a range of debris sizes. In this simulation, the initial configuration of the particle jet was prepared with only two different groups of particle jets; one on the top half with the particle diameter of 5 mm and another at the bottom half with the diameter of 1 mm to demonstrate the effect of the particle sizes on particle precipitation, mixing and sedimentation.

The simulation shows that the smaller particle jet rapidly disintegrated and mixed very well with the large particles during the mixing process. It is also interesting to note that the final configuration of the particle sedimentation showed that the most of small particles settled on the floor by packing the pore generated in between large particles. This occurs since the particles have a regular spherical shape and the thickness of the debris bed on the floor is relatively thin. In a real debris bed where large amount of corium (order of several tens of tons) with a distribution of particle sizes and arbitrary shapes generated during the FCI mixing process, the permeability of those small particles will be very low causing inhomogeneous pore structures in debris bed. Therefore, this simulation results resembles the late-phase settlement of smaller debris generated by the vigorous dynamic interaction during mixing phase on the larger particle bed, causing less permeable debris layer on the top of the debris bed. Both observations: homogeneous mixing and low permeability of small particles, suggested that the porous structure which is important for the cooling pass during coolability could be heterogenous and the surface layer of the debris bed could be less permeable for the surrounding coolant. For the realistic simulation, however, the effects of particle size distributions and shapes as well as vapor plume generated during the boiling process during mixing and settlement of the particle jet will be taken into account in future study.

5. Conclusions

In this paper, the ADDA code with the RD-MPS algorithm was used to simulate the non-boiling Q21 test of the QUEOS experiment in two and three dimensions. The code with a newly enhanced stability of the code numerics and algorithms successfully enables to simulate the entire process of debris bed formation started from the jet breakup, followed by mixing during the particle jet penetration with surrounding liquid, dissipation and precipitation. The simulation showed the characteristic structure of particle jet breakup and mixing with surrounding liquid. The simulation results on the particle jet penetrations, water leveling and the final debris bed formation suggest that for the particle dispersions and precipitation conceiving the debris bed formation and associated coolability analysis, the 2D simulation may be unsuitable to reasonably predict those observed in the 3-D real experiments since the debris bed formation seems largely depending on the process of particle precipitation and mixing phenomena prior to the settlement. The applicability of the simulation for the realistic debris break-up and settlement to form a debris bed was demonstrated by a heterogeneous particle jet with two different particle group sizes. For the realistic simulation, the effects of particle size distributions and shapes as well as vapor plume generated during the boiling process during mixing and settlement of the particle jet will be taken into account in future study.

Acknowledgements

The authors gratefully acknowledge for the support of this work provided by the Ministry of Knowledge Economy in Korea under the project contract of 2010151010001B. The authors also are grateful to Dr. Leonhard Meyer and Dr. Walter Baetz at Karlsruher Institute für Technologie (KIT) for providing the QUEOS experimental information and data.

6. References

[1] N. Reinke, T. Drath, T.v. Berlepsch, H.E. Unger, M.K. Koch, "Formation, Characterization and Cooling of Debris – Scenario Discussion with Emphasis on TMI-2," Nucl. Eng. Des. 236, 2006, pp. 1955-1964.

- [2] D. Magallon, "Characteristics of Corium Debris Beds generated in Large-Scale Fuel-Coolant Interaction Experiments," Nucl. Eng. Des. 236, 2006, pp. 1998-2009.
- [3] M. Bürger, et al., "Coolability of Particulate Beds in Severe Accidents: Status and Remaining Uncertainties," Progress in Nuclear Engineering, 52, 2010, pp. 61-75.
- [4] M.L. Corradini, B.J. Kim, and M.D. Oh, "Steam explosions in Light Water Reactors; A Review of Theory and Modeling," Prog. in Nucl. Ener., Vol. 22, No. 1, 1988, pp. 1-117.
- [5] A. Aziz and A Settari, *Petroleum Reservoir Simulation*, Elsevier Applied Science Publisher, 1985.
- [6] L. Li, A. Karbojian, P. Kudinov and W. Ma, "An Experimental Study on Dryout Heat Flux of Particulate Beds with Irregular Particles," <u>Proc. of ICAPP 2011</u>, Paper 11185, Nice, France, May 2-5, 2011.
- [7] S. Yakush and P. Kudinov, "Effects of Water Pool Subcooling on the Debris Bed Spreading by Coolant Flow," <u>Proc. of ICAPP 2011</u>, Paper 11416, Nice, France, May 2-5, 2011.
- [8] Z. Chen, G. Huan, and Y. Ma., *Computational methods for multiphase flows in porous media*, SIAM Computational Science and Engineering, 2006.
- [9] E. G. Flekkov, G. Wagner and J. Fedar, "Hybrid model for combined particle and continuum dynamics," Europhysics Letters, 52, 2000, pp. 271-276.
- [10] C. Crowe, M. Sommerfeld and Y. Tsuji, *Multiphase flows with droplets and particles*, CRC Press, 1997.
- [11] S. Park, H. S. Park, and G., Jeun, "Simulation of QUEOS Experiment using Rigid Dynamic-Moving Particle Semi-Implicit (RD-MPS) Method," <u>Trans. of the Korean Nuclear Society, Spring Meeting</u>, Taebaek, Korean May 26-27, 2011.
- [12] S. Koshizuka, and Y. Oka, "Moving Particle Semi-implicit Method for Fragmentation of Incompressible Flow, Nucl. Sci. Eng., 123, 1996, pp. 421-434.
- [13] S. Koshizuka, H. Ikeda, Y. Oka, "Numerical Analysis of Fragmentation Mechanisms in Vapor Explosions," Nucl. Eng. Des. 189, 1999, pp. 423–433.
- [14] H. Ikeda, S. Koshizuka, Y. Oka, H. S. Park and J. Sugimoto, "Numerical Analysis of Jet Injection Behavior for Fuel-Coolant Interaction using Particle Method," J. Nucl. Sci. Technol., 38, 3. 2001, pp. 174-182.
- [15] D. Bara, "Curved Surfaces and Coherence for Non-penetrating Rigid Body Simulation," Computer Graphics 24, 4, 1990, pp. 19–28.
- [16] S. Park, and G., Jeun, "Coupling of rigid body dynamics and moving particle semi-implicit method for simulating isothermal multi-phase fluid interactions," Comput. Methods Appl. Mech. Eng., Vol. 200, Issues 1-4, 2011, pp. 130-140.
- [17] L. Meyer, and G. Schumacher, "QUEOS, A Simulation-Experiment of the Premixing Phase of a Steam Explosion with Hot Spheres in Water: Based Case Experiments," FZKA 5612, Forschungszentrum Karsruhe, German, 1996.
- [18] L. Meyer, "QUEOS, A Simulation-Experiment of the Premixing Phase of a Steam Explosion with Hot Spheres in Water: Results of the Second Test Series," INR Nr. 1692/97, PSF-Nr. 3267, Forschungszentrum Karsruhe, German, 1997.